



Leaky-Wave Antenna With Alternately Loaded Complementary Radiation Elements

Yue-Long Lyu , *Student Member, IEEE*, Fan-Yi Meng , *Senior Member, IEEE*, Guo-Hui Yang, *Member, IEEE*, Qun Wu, *Senior Member, IEEE*, and Ke Wu , *Fellow, IEEE*

Abstract—In this letter, we compare the scanning beams of two leaky-wave antennas (LWAs), respectively, loaded with capacitive and inductive radiation elements, which have not been fully discussed in previous publications. It is pointed out that an LWA with only one type of radiation element suffers from a significant gain fluctuation over its beam-scanning band. To remedy this problem, we propose an LWA alternately loaded with inductive and capacitive elements along the host transmission line. The proposed LWA is able to steer its beam continuously from backward to forward with constant gain. A microstrip-based LWA is designed on the basis of the proposed method, and the measurement of its fabricated prototype demonstrates and confirms the desired results. This design method can widely be used to obtain LWAs with constant gain based on a variety of TLs.

Index Terms—Complementary radiation elements, constant gain, leaky-wave antenna (LWA).

I. INTRODUCTION

LEAKY-WAVE antennas (LWAs) are widely investigated traveling-wave radiating structures that can support unique beam scanning with high directivity [1], [2]. In fact, LWAs may be considered as feeder-integrated array antennas. In an LWA, radiation elements can be periodically distributed along a transmission line (TL), and this kind of LWA is referred to as periodic LWA (PLWA), featuring both backward and forward beam scanning [1]. Moreover, one can also design PLWAs with broadside radiation by applying design methods, which can suppress the open-stopband (OSB) effect, such as the use of reflection cancellation structure [3], asymmetric geometry [4]–[6], impedance-matched unit cell [3], [7]–[10], and alternately cascading TL segments of two types [11]. The LWA radiation elements of almost all kinds are nonresonant, i.e., inductive or capacitive. However, most of the LWAs have only one type of radiation element, which suffers from a significant

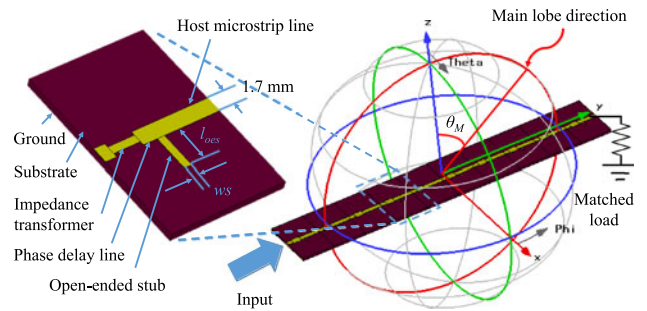


Fig. 1. Geometry of the LWA based on microstrip line with open-ended stubs designed according to [3].

gain fluctuation over the operation band [8], as discussed later in this letter. On the contrary, constant gain with respect to frequency can be achieved by using wideband radiators in LWAs [12], [13]. However, the lower and upper boundaries of beam-scanning frequency band of these LWAs cannot be easily and independently controlled because the wideband radiators within these LWAs feature relatively complex physical structures.

In this letter, radiation properties of LWAs proposed in [3] are further investigated in Section II. It is found out that the LWA with shunt capacitive radiation elements and the LWA with shunt inductive radiation elements feature complementary radiation efficiency variations with respect to frequency. Thus, in Section III, a supercell is designed by cascading two subunit cells with capacitive and inductive radiation elements, respectively. The proposed supercell features a constant high-radiation efficiency over the entire operation band, and hence the LWA composed of the supercells is able to radiate continuous scanning beam from backward to forward with a constant gain. Moreover, the two types of subunit cells in the proposed LWA have simple structures and can be optimized individually, which means flexible radiation property control is achievable. An LWA prototype is fabricated and measured. The measured results verify the simulated results well.

II. LWAS WITH CAPACITIVE OR INDUCTIVE RADIATION ELEMENTS

In [3], a series of LWAs is designed by loading open-ended stubs on a microstrip line, as shown in Fig. 1. Utilizing a phase delay line and an impedance transformer, OSB can be suppressed, and thus a broadside radiation can be obtained. In this letter, RO3035 ($\epsilon_r = 3.5$, $\tan \delta = 0.0015$) with thickness of 0.762 mm is used as a substrate material. The host microstrip line is 1.7 mm wide with characteristic impedance of 50 Ω .

Manuscript received February 9, 2018; revised February 26, 2018; accepted February 28, 2018. Date of publication March 8, 2018; date of current version April 5, 2018. This work was supported in part by the National Natural Science Foundation of China under Grant 61671180 and Grant 61501275, and in part by the Science Foundation Project of Heilongjiang Province of China under Grant QC2015073. (Corresponding authors: Fan-Yi Meng; Ke Wu.)

Y.-L. Lyu is with the Department of Microwave Engineering, Harbin Institute of Technology, Harbin 150001, China, and also with the Poly-Grames Research Center, Polytechnique Montréal, Montréal, QC H3T 1J4, Canada (e-mail: lvyuelonglvyuelong@126.com).

F.-Y. Meng, G.-H. Yang, and Q. Wu are with the Department of Microwave Engineering, Harbin Institute of Technology, Harbin 150001, China (e-mail: blade@hit.edu.cn; gh.yang@hit.edu.cn; qwu@hit.edu.cn).

K. Wu is with the Poly-Grames Research Center, Polytechnique Montréal, Montréal, QC H3T 1J4, Canada (e-mail: ke.wu@polymtl.ca).

Digital Object Identifier 10.1109/LAWP.2018.2811726

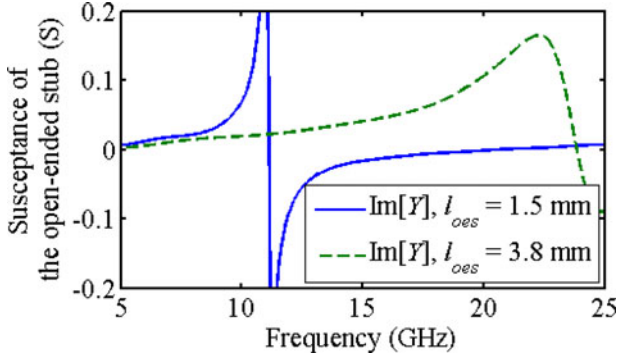


Fig. 2. Simulated susceptances of open-ended stubs.

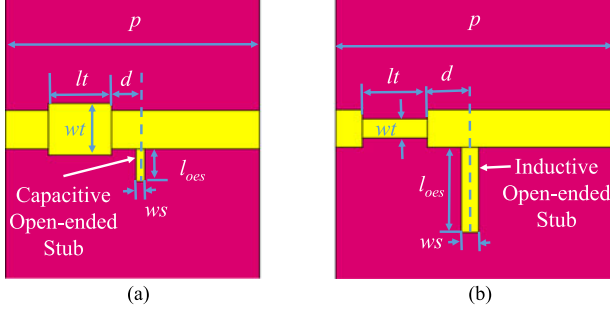


Fig. 3. LWA unit cells containing (a) capacitive radiation element and (b) inductive radiation element, respectively.

The broadside radiation frequency, i.e., the transition frequency is designed at 15 GHz. All the numerical simulations are conducted in CST MWS. The length l_{oes} of the open-ended stub is a key parameter in the design of the total LWA as it determines the admittance of the open-ended stub. However, the effect of l_{oes} on the radiation properties of the total LWA was not discussed in [3].

When the loaded open-ended stub is shorter than a quarter-waveguide wavelength, it introduces a shunt capacitance to the equivalent circuit of the LWA unit cell. For example, when $l_{oes} = 1.5$ mm, the stub is capacitive in the frequency band from 5 to 24 GHz, as shown in Fig. 2, where the extracted imaginary part of the admittance Y of the open-ended stub from numerical simulation is plotted. When the loaded open-ended stub is shorter than half a waveguide wavelength and longer than a quarter-waveguide wavelength at 15 GHz, it acts as a shunt inductor in the equivalent circuit of the LWA unit cell. As shown in Fig. 2, the susceptance of an open-ended stub of 3.8 mm length is negative from 11 to 21 GHz, indicating that this open-ended stub is inductive in this band.

The parameter values of the phase delay line and transformer can be obtained according to the design procedure in [3]. For the case of a unit cell containing a capacitive radiation element, the quarter-wave impedance transformer should be wider than the host microstrip line, as shown in Fig. 3(a). On the contrary, the quarter-wave impedance transformer is narrower than the host microstrip line in the LWA unit cell containing an inductive open-ended stub, as shown in Fig. 3(b).

With $l_{oes} = 1.5$ mm or $l_{oes} = 3.8$ mm, other parameters of the LWA unit cell labeled in Fig. 3 can be easily obtained to achieve the broadside radiation at 15 GHz through numerical simulations, and the optimized values are tabulated in Table I. The unit

TABLE I
PARAMETER VALUES (mm)

	l_{oes}	ws	D	lt	wt	p
Unit cell #1	1.5	0.4	1.3	2.8	2.3	11.3
Unit cell #2	3.8	0.8	1.9	2.9	0.85	12.5

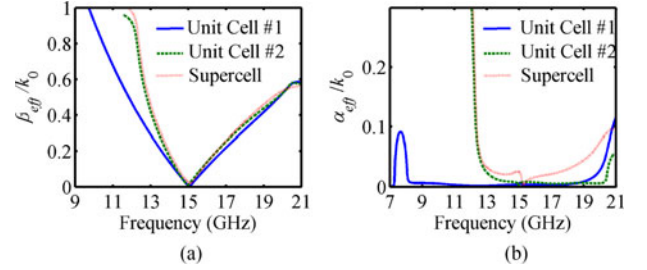


Fig. 4. Normalized simulated (a) phase and (b) attenuation constants of unit cells #1, #2, and the proposed supercell.

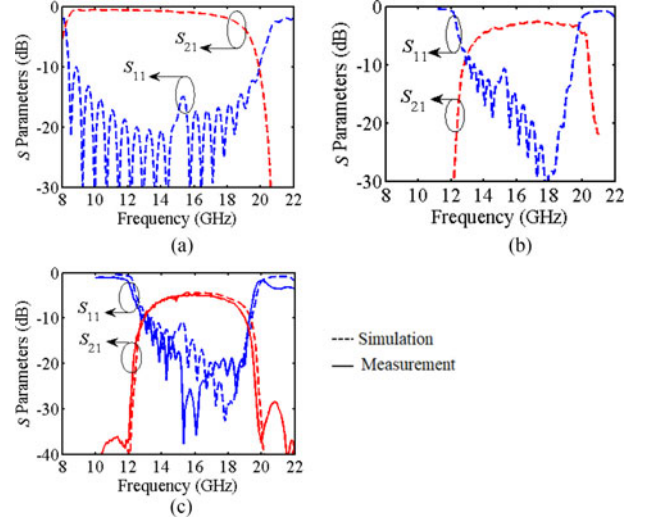


Fig. 5. Simulated S -parameters of (a) LWA #1, (b) LWA #2, and (c) LWA #3 (along with the measured results).

cell with $l_{oes} = 1.5$ mm is referred to as unit cell #1, whereas the unit cell with $l_{oes} = 3.8$ mm is referred to as unit cell #2. In total, ten unit cells #1 are cascaded to form an LWA, which is labeled as LWA #1, and the other LWA, labeled as LWA #2, is obtained by cascading ten unit cells #2. The dispersion diagrams (extracted normalized effective phase constant β_{eff}/k_0 and normalized attenuation constant α_{eff}/k_0 , where k_0 is the wavenumber of free space) of unit cells #1 and #2 are plotted in Fig. 4.

It can be inferred from Fig. 4 that beam scanning of LWA #1 will occur in the band from 9.5 to 20 GHz where $\beta_{eff} < k_0$ and α_{eff} is small enough [1]. As shown in Fig. 5(a), the simulated $|S_{11}|$ of LWA #1 is smaller than -10 dB in this band, including the transition frequency of 15 GHz, which means the OSB is well suppressed. Beam scanning occurs in the fast-wave region of a passband between the adjacent closed stopbands, where $\beta_{eff} \cdot p = -(2n + 1)\pi$, $n = 0, \pm 1, \pm 2$, [1]. The upper boundary of the beam-scanning band of LWA #1 is mainly determined by the length of the capacitive open-ended stubs as an

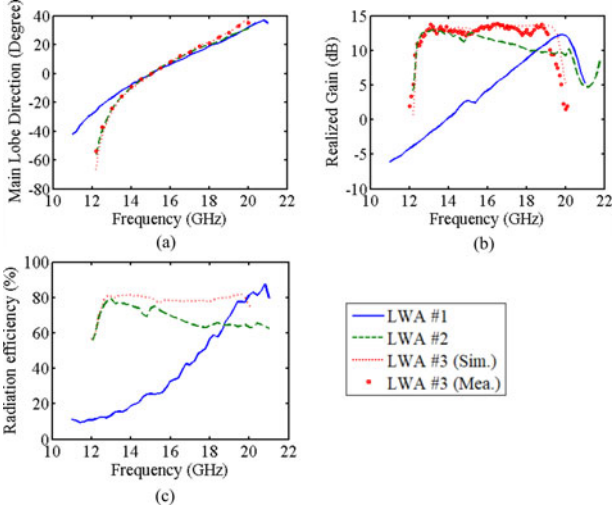


Fig. 6. Simulated radiation properties of LWA #1, LWA #2, and LWA #3, where (a) demonstrates the main lobe direction (compared with the measured results of LWA #3), (b) shows the realized gain (compared with the measured results of LWA #3), and (c) plots the radiation efficiency.

open-ended stub causes large phase delay near the frequency where its electric length is $\pi/2$ (at about 24 GHz for the case of $l_{\text{oes}} = 1.5$ mm, as shown in Fig. 2), whereas the lower boundary is mainly determined by the phase delay of the host TL segments with space harmonic order of -1 [1]. Therefore, the length of the capacitive open-ended stubs can be adjusted to effectively control the bandwidth of the forward beam scanning of LWA #1. We can obtain LWA #1 with a narrower forward beam-scanning band by increasing the length of the capacitive open-ended stubs. It should also be noted that longer capacitive open-ended stubs also lead to wider impedance transformers, which would cause higher cross-polarization level.

For the case of unit cell #2 and LWA #2, beam-scanning band starts from 13 GHz and ends at 20 GHz, according to Fig. 4. In this band, the simulated $|S_{11}|$ of LWA #2 is smaller than -10 dB as shown in Fig. 5(b). Return loss of LWA #2 is also larger than 10 dB at 15 GHz. Contrary to the case of unit cell #1 and LWA #1, the length of the loaded open-ended stubs (the inductive stubs) significantly affects the lower boundary of the beam-scanning band. An LWA #2 with longer inductive stubs features a wider backward beam-scanning band. Moreover, as the width wt of the impedance transformer in a unit cell #2 with a longer inductive stub is accordingly closer to that of the host TL, the cross-polarization level of the LWA #2 with longer inductive stubs is hence lower.

On the other hand, as shown in Fig. 5(a), $|S_{21}|$ of LWA #1 decreases slowly with the increasing frequency, which means that the residual power flowing out of LWA #1 is smaller at higher frequencies of the operation band. On the contrary, residual power flowing out of LWA #2 is smaller at lower frequencies as shown in Fig. 5(b).

The main lobe directions of LWA #1 and LWA #2 are simulated and illustrated in Fig. 6(a). It can be observed that both LWAs are able to steer their beams from backward through broadside and then to forward continuously. However, both LWA #1 and LWA #2 feature a significant gain fluctuation versus frequency, as shown in Fig. 6(b), where the realized gain of LWA #1 and LWA #2 increases and decreases as frequency goes up,

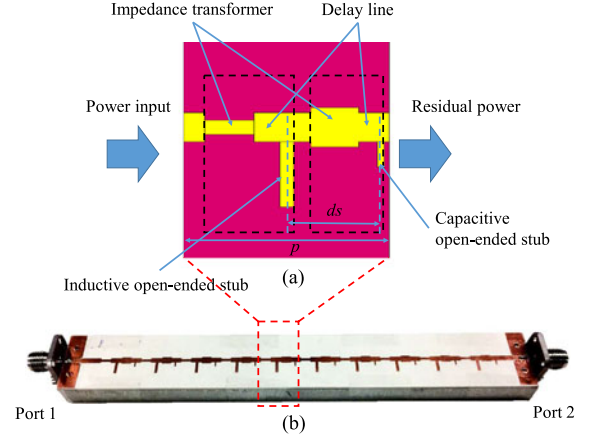


Fig. 7. (a) Geometry of the supercell composed of both capacitive and inductive radiation elements, where $ds = 5.5$ mm and $p = 12$ mm, and (b) photograph of the prototype of an LWA constructed by cascading ten proposed supercells.

respectively. The significant gain fluctuation over the operation band stems from the dramatically varying radiation efficiency over frequency [see in Fig. 6(c)]. It is worth noting that as the effective aperture of LWA #2 increases with frequency, its gain fluctuation over frequency is mitigated and not as significant as its counterpart of LWA #1. Although both LWA #1 and LWA #2 feature a frequency-gain fluctuation, their radiation performances with respect to frequency are complementary, which means that an LWA designed with both types of radiation elements, which will be demonstrated in Section III, is promising to obtain a constant gain over the entire operation band.

III. LWA WITH BOTH CAPACITIVE AND INDUCTIVE RADIATION ELEMENTS

In order to utilize both inductive and capacitive radiation elements within one LWA, a supercell constructed by cascading a unit cell #1 and a unit cell #2 is proposed as shown in Fig. 7(a). The parameter values of the radiation stubs and their corresponding phase delay lines and impedance transformers are the same as in Section II. As the signs of the susceptances of the open-ended stubs in the proposed supercell are opposite to each other, the currents on the two stubs will flow along opposite directions about the host microstrip line when the two stubs are excited by microwave power with the same phase. In order to make the two open-ended stubs radiate power in phase, distance ds between the two stubs should be optimized to introduce a proper additional phase difference between the currents on the two stubs. The period p of the supercell should be optimized to obtain a phase delay of the supercell of 2π at 15 GHz for broadside radiation of the total LWA. The final parameter values of p and ds of the supercell are listed in the caption of Fig. 7.

Simulated current distributions on the surface of the supercell at several frequencies are illustrated in Fig. 8. It can be observed that the currents on the stubs flow along the same direction. Moreover, at 13 GHz, currents on the inductive stub are much stronger than those on the capacitive stub, which is contrary to the case for 17 GHz. Therefore, the supercell is able to radiate effectively over the entire operation frequency band due to the complementary radiation performances of the two stubs, mean-

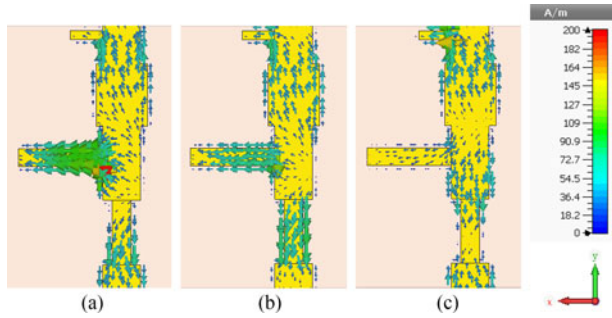


Fig. 8. Simulated surface current distributions on the supercell at (a) 13, (b) 15, and (c) 17 GHz.

ing that a constant radiation efficiency can be obtained using the proposed supercell with proper parameter values.

The extracted simulated β_{eff} and α_{eff} of the supercell are depicted in Fig. 4(a) and (b), respectively. It can be observed that lower boundary of the operation band of the proposed supercell is almost the same as that of unit cell #2, whereas the upper boundary is similar to those of unit cell #1 and unit cell #2. Ten supercells are cascaded to form an LWA, referred to as LWA #3. Simulated S -parameters of LWA #3 are depicted in Fig. 5(c). The passband of LWA #3 ($|S_{11}| < -10$ dB) begins at 13 GHz and ends at 19.45 GHz, which is the intersection of those of LWA #1 and LWA #2. $|S_{11}|$ of LWA #3 at 15 GHz can be further decreased by suppressing the fluctuation of α_{eff} around transition frequency shown in Fig. 4(b) with iterated impedance matching according to [3]. As discussed in Section II, the upper band boundary of LWA #1 and the lower band boundary of LWA #2 are mainly determined by the lengths of the capacitive and inductive stubs, respectively. Therefore, both the lower and upper band boundaries of the proposed supercell can be relatively freely controlled by individually designing unit cells #1 and #2 with desired upper and lower band boundaries, respectively, which is very useful in practical application scenarios such as radar systems. Simulated radiation properties of LWA #3 are also illustrated in Fig. 6. As shown in Fig. 6(a), LWA #3 steers its beam from backward to forward smoothly within its passband. Compared with the cases of LWA #1 and LWA #2, the scanning beam of LWA #3 features a constant gain as described in Fig. 6(b). The beam-scanning range with gain fluctuation smaller than 3 dB is from -48° to 35° . The constant gain stems from the constant radiation efficiency of LWA #3 as, shown in Fig. 6(c).

To verify the simulated results, a prototype of LWA #3, shown in Fig. 7(b), is manufactured and experimentally measured. The measured S -parameters, along with the corresponding simulated data, are depicted in Fig. 5(c). The prototype is also measured in an anechoic chamber, where the prototype is fed through port 1 and connected with a matched load of 50Ω through port 2. The measured main lobe direction, and realized gain are added in Fig. 6(a) and (b), respectively, for comparison. All the measured results demonstrate a reasonable agreement with the simulated data. The measured radiation patterns in the elevation plane (H plane) at several frequency samples are depicted in Fig. 9, with corresponding simulated results for comparison. Only small discrepancies between the measured and simulated results can be found. It can be observed in Fig. 9 that the cross-polarization level of the prototype is near -10 dB over the operation band. As discussed earlier in this letter, the

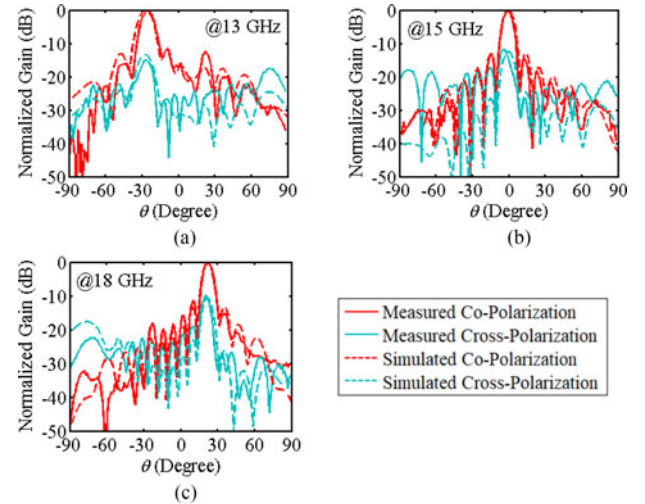


Fig. 9. Measured and simulated radiation patterns of the prototype at (a) 13, (b) 15, and (c) 18 GHz.

frequency-scanning cross-polarization beam is leaked through the discontinuities of the impedance transformers in the supercells [14]. Once the prototype is designed with larger beam-scanning bandwidth, its cross-polarization level would be reduced. Moreover, using TL with closed structure is also helpful to suppress cross-polarization, such as the half-mode substrate-integrated waveguide (HM SIW) used in [13].

IV. DISCUSSION

Actually, LWAs with constant gain with respect to frequency can also be designed with other types of radiation elements and TLs, such as SIW with both inductive and capacitive slots, coplanar waveguide with both gaps and slits analyzed in [15], etc., only if the radiation elements feature complementary radiation performances versus frequency. Moreover, it is also true that series inductive or capacitive radiation elements in an LWA demonstrate increasing or decreasing radiation efficiency with respect to frequency, such as the series capacitive slots in [16] and the series inductive slots in [9]. Using both series inductive and capacitive radiation elements properly is also promising to obtain LWA with constant gain versus frequency.

V. CONCLUSION

In this letter, it is found that LWAs with capacitive or inductive radiation elements suffer from gain variation over frequency. An LWA is hence designed by alternately cascading unit cells with capacitive and inductive radiation elements. The proposed LWA features relatively high and constant gain within its beam-scanning band due to the radiation complementarity of the two types of radiation elements. A prototype designed based on microstrip line techniques is demonstrated with confirming favored results.

REFERENCES

- [1] A. A. Oliner and D. R. Jackson, *Antenna Engineering Hand Book*, 4th ed. New York, NY, USA: McGraw-Hill, 2007.
- [2] F. Xu and K. Wu, "Understanding leaky-wave structures: A special form of guided-wave structure," *IEEE Microw. Mag.*, vol. 14, no. 5, pp. 87–96, Jul./Aug. 2013.

- [3] S. Paulotto, P. Baccarelli, F. Frezza, and D. R. Jackson, "A novel technique for open-stopband suppression in 1-D periodic printed leaky-wave antennas," *IEEE Trans. Antennas Propag.*, vol. 57, no. 7, pp. 1894–1906, Jul. 2009.
- [4] S. Otto, A. Al-Bassam, A. Rennings, K. Solbach, and C. Caloz, "Transversal asymmetry in periodic leaky-wave antennas for Bloch impedance and radiation efficiency equalization through broadside," *IEEE Trans. Antennas Propag.*, vol. 62, no. 10, pp. 5037–5054, Oct. 2014.
- [5] S. Otto, C. Zhichao, A. Al-Bassam, A. Rennings, K. Solbach, and C. Caloz, "Circular polarization of periodic leaky-wave antennas with axial asymmetry: Theoretical proof and experimental demonstration," *IEEE Trans. Antennas Propag.*, vol. 62, no. 4, pp. 1817–1829, Apr. 2014.
- [6] D. Ye, Y. Li, Z. Liang, J. Liu, S. Zheng, and Y. Long, "Periodic triangle-truncated DSPSL-based antenna with backfire to endfire beam-scanning capacity," *IEEE Trans. Antennas Propag.*, vol. 65, no. 2, pp. 845–849, Feb. 2017.
- [7] N. Yang, C. Caloz, and K. Wu, "Full-space scanning periodic phase-reversal leaky-wave antenna," *IEEE Trans. Microw. Theory Techn.*, vol. 58, no. 10, pp. 2619–2632, Oct. 2010.
- [8] Y. L. Lyu *et al.*, "Leaky-wave antennas based on noncutoff substrate integrated waveguide supporting beam scanning from backward to forward," *IEEE Trans. Antennas Propag.*, vol. 64, no. 6, pp. 2155–2164, Jun. 2016.
- [9] Y. L. Lyu, F. Y. Meng, G. H. Yang, D. Erni, Q. Wu, and K. Wu, "Periodic SIW leaky-wave antenna with large circularly polarized beam scanning range," *IEEE Antennas Wireless Propag. Lett.*, vol. 16, pp. 2493–2496, 2017.
- [10] J. T. Williams, P. Baccarelli, S. Paulotto, and D. R. Jackson, "1-D combline leaky-wave antenna with the open-stopband suppressed: Design considerations and comparisons with measurements," *IEEE Trans. Antennas Propag.*, vol. 61, no. 9, pp. 4484–4492, Sep. 2013.
- [11] D. Xie *et al.*, "Uniform periodic leaky-wave antennas with eliminated open stopbands," *IEEE Antennas Wireless Propag. Lett.*, vol. 16, pp. 2110–2113, 2017.
- [12] S. Paulotto, P. Baccarelli, and D. R. Jackson, "A self-matched wide scanning U-stub microstrip periodic leaky-wave antenna," *J. Electromagn. Waves Appl.*, vol. 28, pp. 151–164, Jan. 2014.
- [13] R. Henry and M. Okoniewski, "A broadside scanning substrate integrated waveguide periodic phase-reversal leaky-wave antenna," *IEEE Antennas Wireless Propag. Lett.*, vol. 15, pp. 602–605, 2016.
- [14] Z. L. Ma and L. J. Jiang, "One-dimensional triple periodic dual-beam microstrip leaky-wave antenna," *IEEE Antennas Wireless Propag. Lett.*, vol. 14, pp. 390–393, 2015.
- [15] Z. Lei and W. Ke, "Characterization of finite-ground CPW reactive series-connected elements for innovative design of uniplanar M(H)MICs," *IEEE Trans. Microw. Theory Techn.*, vol. 50, no. 2, pp. 549–557, Feb. 2002.
- [16] Y. D. Dong and T. Itoh, "Composite right/left-handed substrate integrated waveguide and half mode substrate integrated waveguide leaky-wave structures," *IEEE Trans. Antennas Propag.*, vol. 59, no. 3, pp. 767–775, Mar. 2011.